JGR Solid Earth

RESEARCH ARTICLE
10.1029/2020JB021499

Special Section:
Machine learning for Solid Earth observation, modeling and understanding

Predicting Geothermal Heat Flow in Antarctica With a Machine Learning Approach

M. Lösing[1] and **J. Ebbing**[1]

[1]Institute of Geosciences, Kiel University, Kiel, Germany

Key Points:

- A new geothermal heat flow map of Antarctica is established by adopting a machine learning approach
- Input features include both global and regional geological and tectonic information, and heat flow observations
- A Gondwana reconstruction shows connections of heat flow at the conjugate margins of East Antarctica

Supporting Information:

Supporting Information may be found in the online version of this article.

Correspondence to:

M. Lösing,
mareen.loesing@ifg.uni-kiel.de

Citation:

Lösing, M., & Ebbing, J. (2021). Predicting geothermal heat flow in Antarctica with a machine learning approach. *Journal of Geophysical Research: Solid Earth*, *126*, e2020JB021499. https://doi.org/10.1029/2020JB021499

Received 8 DEC 2020
Accepted 24 MAY 2021

Abstract We present a machine learning approach to statistically derive geothermal heat flow (GHF) for Antarctica. The adopted approach estimates GHF from multiple geophysical and geological data sets, assuming that GHF is substantially related to the geodynamic setting of the plates. We apply a Gradient Boosted Regression Tree algorithm to find an optimal prediction model relating GHF to the observables. The geophysical and geological features are primarily global data sets, which are often unreliable in polar regions due to limited data coverage. Quality and reliability of the data sets are reviewed and discussed in line with the estimated GHF model. Predictions for Australia, where an extensive database of GHF measurements exists, demonstrate the validity of the approach. In Antarctica, only a sparse number of direct GHF measurements are available. Therefore, we explore the use of regional data sets of Antarctica and its tectonic Gondwana neighbors to refine the predictions. With this, we demonstrate the need for adding reliable data to the machine learning approach. Finally, we present a new geothermal heat flow map, which exhibits intermediate values compared to previous models, ranging from 35 to 156 mW/m^2, and visible connections to the conjugate margins in Australia, Africa, and India.

Plain Language Summary The heat energy transferred from the Earth's interior to the surface (geothermal heat flow) can substantially affect the dynamics of an overlying ice sheet. It can lead to melting at the base and hence, decouple the ice sheet from the bedrock. In Antarctica, this parameter is poorly constrained, and only a sparse number of thermal gradient measurements exist. Indirect methods, therefore, try to estimate the continental Antarctic heat flow. Here, we use a machine learning approach to combine multiple information on geology, tectonic setting, and heat flow measurements from all continents to predict Antarctic values. We further show that using reliable data is crucial for the resulting prediction and a mindful choice of features is recommendable. The final result exhibits values within the range of previously proposed heat flow maps and shows local similarities to the continents once connected to East Antarctica within the supercontinent Gondwana. We suggest a minimum and maximum heat flow map, which can be used as input for ice sheet modeling and sea level rise predictions.

1. Introduction

GHF is a crucial and poorly constrained parameter for ice sheet modeling, and hence glacial isostatic adjustment calculations. It affects the ice rheology and can lead to basal melting, thereby promoting ice flow (e.g., Larour et al., 2012; Pittard et al., 2016; Winsborrow et al., 2010). A difference of 20 mW/m^2 can already increase the basal melt rate from 6.7 to 18 km^3/yr (Llubes et al., 2006).

In-situ observations from temperature gradient measurements are sparse and go along with several uncertainties like climatic changes or hydrothermal circulation (Burton-Johnson et al., 2020).

To establish continent-wide heat flow models, one must refer to indirect methods using geophysical or geological data. The results differ immensely, for example, between magnetic and seismological data (e.g., An et al., 2015b; Martos et al., 2017), and the underlying assumptions cannot be easily combined (Lösing et al., 2020). While these different approaches usually take the respective sensitivity ranges into account, simplifications like a definition of laterally constant thermal parameters are not considered in the assessment. Recently, Shen et al. (2020) demonstrated how an updated seismic tomography model completely changed the estimated GHF and its uncertainties compared to earlier studies by Shapiro and Ritzwoller (2004). In ice-covered regions, different geophysical models show no consensus on magnitude and spatial distribution of heat flow (Rezvanbehbahani et al., 2019; Van Liefferinge, 2018).

Alternatively, statistical analysis (Goutorbe et al., 2011; Lucazeau, 2019) can be used to establish global models of GHF. Various features deemed appropriate for heat flow characterization are used to predict GHF in areas not covered with measurements. The known values are extrapolated to regions with a similar geological setting, often relying on global data sets. For example, Lucazeau (2019) presented a new global GHF model by empirically selecting an optimum of 14 geological and geophysical observables. However, global maps often lack information in ice-covered regions and are mostly just interpolated into these areas. Therefore, the results from these studies might be a simplification for Antarctica, and an empirical decision might not necessarily be the right choice.

A promising alternative has been presented by Rezvanbehbahani et al. (2017) for estimating GHF in Greenland. In their study, they use a machine learning algorithm to find the optimal predictors. However, some features might not be meaningful for polar regions or are overrepresented.

As in the study for Greenland, we apply a supervised machine learning regression approach with a more thorough choice of data sets. We use a slightly enhanced implementation and geological features from various global and regional model to evaluate the influence of the input data. Furthermore, we use combined heat flow data from three different data sets, including a thoroughly compiled database for Antarctica (Burton-Johnson et al., 2020). As a result, we test the method's performance on the geophysically well-known continent Australia and present a new heat flow map for Antarctica.

2. Method

To make quantitative predictions, a regression algorithm that captures the complex linkages between heat flow and its geological environment is required. For this, we use gradient boosting regression, a supervised machine learning technique, which iteratively creates an ensemble of regression trees. Each tree additively fits to the loss function gradient of the previous (Friedman, 2001). Rezvanbehbahani et al. (2017) already give a comprehensive mathematical description with the application to heat flow and geological data.

The advantage of regression trees is that they are able to capture nonlinear relationships by doing recursive partitioning of the data with logical splitting conditions. Therefore, the algorithm walks through every feature to find the best threshold for splitting, constrained by some user-defined criteria like the maximum depth, maximum number of leaves, and minimum samples per leaf of the tree. At each iteration of the gradient boosting procedure, a tree is trained on a subset of the data to predict the steepest gradient descent step. In contrast to gradient descent, which optimizes the model parameters, gradient boosting optimizes (boosts) the model or tree itself. Saving the trees as an ensemble model in memory enables to output predictions for any future sample. Unlike, for example, neural networks, the regression trees are traceable and easy to interpret.

2.1. Regularized Tree Boosting: *XGBoost*

We use an advanced and more regularized implementation of gradient boosting regression, the open-source library *XGBoost* (Chen & Guestrin, 2016), provided among others for Python, which is highly efficient in its performance. Some of the advantages are the possibility of regularization, stochastic subsampling, parallel processing, and built-in cross-validation for parameter tuning. For example, the algorithm can prune a tree backward and remove splits that are beyond positive gain. In contrast to basic gradient boosting, this implementation would not stop splitting upon the first negative loss but go deeper if positive loss follows.

The goal is to find the best tree model that fits the training data x_i and target values y_i. The quality of the established model is then reviewed by a defined objective function (Chen & Guestrin, 2016)

$$obj = \sum_{i=1}^{n} L(y_i, \hat{y}_i) + \sum_{k=1}^{K} \Omega(f_k), \tag{1}$$

$$\Omega(f) = \gamma T + \frac{1}{2}\lambda \parallel w \parallel^2,$$

where n is the number of training values and K is the number of trees. L is the loss function that measures how well the model explains the training data by comparing them to the predicted values $\hat{y}_i$. Ω is the regularization term that regulates the complexity of the tree f_k. Each f_k is defined by an independent tree structure q and leaf weights w with $f_k \in \mathcal{F}$ where $\mathcal{F} = \{f(x)=w_{q(x)}\}$ is a space of functions containing all regression trees. The first term of Ω, where T is the number of leaves and γ is a penalization factor, is responsible for tree pruning and can reduce overfitting. In the second $L2$ regularization term λ scales the sensitivity of the prediction to individual observations.

In order to find the optimal tree, the objective function needs to be optimized. *XGBoost* therefore uses the Newton method by applying a second-order Taylor approximation of the objective function (Equation 1) providing an enhanced estimation of the highest minimization direction. Defining the gradient of the loss function as $g_i = \partial_{\hat{y}^{(t-1)}} L(y_i, \hat{y}^{(t-1)})$ and the Hessian as $h_i = \partial^2_{\hat{y}^{(t-1)}} L(y_i, \hat{y}^{(t-1)})$, where t represents a certain stage of the training, and removing constant terms the objective function changes to

$$obj^{(t)} \simeq \sum_{i=1}^{n} \left[g_i f_t(x_i) + \frac{1}{2} h_i f_t^2(x_i) \right] + \Omega(f_t).$$

Further overfitting is prevented by introducing a shrinkage that scales every new tree added to the model by a factor ϵ. It, therefore, controls the influence of an individual tree, and empirical studies showed that small values ($\epsilon \leq 0.1$) lead to better predictions (Friedman, 2001).

2.2. Final Model Evaluation

The data are divided into a training and a test set. The former is used to build the final model, which is then validated to the test data. Here, we use squared errors as loss function and a fivefold grid-search to find the optimal values for shrinkage, maximum tree depth, and subsampling. A quantitative model evaluation is carried out analogous to Rezvanbehbahani et al. (2017) by calculating the normalized root-mean-square error (RMSE/mean) of the test set and the model score and R^2 score, which are relative measures for how well the model explains the variability between observed and predicted train and test values, respectively.

For our analysis, we split the available observed heat flow values randomly into 80% training and 20% test data, but make sure that all Antarctic measurements are within the training data set. According to Rezvanbehbahani et al. (2017), the prediction accuracy improves by increasing the number of samples from the region of interest within the training set. The grid-search results in a shrinkage of $\epsilon = 0.01$ for $K = 1{,}000$, a maximum tree depth of 11 vertices, a subsampling of 0.7, meaning that prior to building a tree, the training data are further split up and only 70% of the data are used. We chose $\gamma = 120$ and keep the default value $\lambda = 1$.

Furthermore, the importance of an individual feature for the model is calculated for every tree and subsequently averaged over the whole model. It describes the reduction of uncertainty of the target values y_i provided by each attribute split point and is weighted by the number of observations in the respective node. Consequently, the feature becomes more important when it is essential for reducing the loss function and, therefore, contributes to improving the prediction model. Highly correlated input features can lead to an improper interpretation of their respective relevance. The split points might be chosen equally often between these features, thereby decreasing their associated importance. Reducing the number of strongly correlated features is, therefore, essential for a sensible analysis.

3. Data

In the following, we present the data that are used for model construction. As target values y_i we use a GHF measurement compilation from three different databases and for the predictor variables x_i, we suggest a number of geological features, which are linked to each GHF value.

Table 1
The Geophysical and Geological Features Used in This Study With Their Respective Sources

	Feature	Publication
1	Moho depth	Szwillus et al. (2019)
	Antarctic Moho depth	An et al. (2015a) and Pappa et al. (2019)
	Australian Moho depth	Kennett et al. (2018)
	African Moho depth	Youssof et al. (2013)
2	LAB depth	Afonso et al. (2019)
	Antarctic LAB depth	An et al. (2015b) and Pappa et al. (2019)
3	Topography	Hirt and Rexer (2015) and Morlighem et al. (2020)
4	Susceptibility	Inferred from Hemant and Maus (2005)
5	Tectonic units	Schaeffer and Lebedev (2015)
6	Gravity mean curvature	Ebbing et al. (2018)
7	Vertical magnetic field	Ebbing et al. (2021)
8	Distance to ridges	Coffin et al. (1997)
9	Distance to trenches	Coffin et al. (1997)
10	Distance to transform faults	Coffin et al. (1997)
11	Distance to young rifts	Şengör and Natal'in (2001)
12	Distance to volcanoes and van Wyk de Vries et al. (2018)	Global Volcanism Program (2013)

3.1. Geothermal Heat Flow

Global GHF measurements are available on http://heatflow.org/ (Hasterok, 2019). We complemented this data set with the database from Lucazeau (2019) and for Antarctica, we explicitly used the revised data set from Burton-Johnson et al. (2020). It is important to mention that these thermal gradient measurements can only be understood as estimates of GHF because several processes might influence the result, for example, surface temperature variation and hydrothermal circulation.

Anomalously high values (>200 mW/m^2) are assumed to be not representative of a whole continent, but related to local geothermal processes ($10^0 - 10^1$ km, Bachu, 1988) and, therefore, not considered in our statistical analysis. In Antarctica, they are also associated with low quality and appear to be exceptional (Figure S1). GHF can vary significantly over a lateral spatial resolution of ~10 km. Employing a relatively high model resolution of 0.25° lead to artifacts and strong gradients in the predicted heat flow map, which is partly related to the low resolution of the global data sets. Therefore, we scaled the resolution down to 0.5° which appears sufficient to resolve the continental trends. As we concentrate on Antarctica, we excluded marine measurements and all measurements assigned the quality "D: Data not used in heat flow maps" according to Lucazeau (2019). As a consequence, the global ~70,000 measurements are reduced to ~10,000 after filtering, binning, and limiting to continental data (>1,000 m below sea level). The mean heat flow of the remaining measurements is 64 mW/m^2 with a standard deviation of 25.6 mW/m^2 (Figures S2 and S3).

3.2. Geological and Geophysical Information

Data used for the model prediction need to be selected carefully and only features with a possible relation to heat flow are useful (Table 1). Furthermore, we tried to use data sets where independent information are included to prevent possible biases and global maps with homogeneous coverage. Some of the data sets used in earlier studies are quite unreliable for Antarctica or superseded by efforts to incorporate local data in recent years. A model built on information that is not available or associated with high errors in the region of interest is impractical. Therefore, we only chose data sets that include reliable data for Antarctica.

The crustal thickness is an essential parameter for heat flow estimation. We used a kriging interpolation of different Moho depths, which was compiled using active source seismic data (Szwillus et al., 2019) incorporating available seismic stations for Antarctica from the USGS GSC database (Mooney, 2015). In contrast

to CRUST1.0 (Laske et al., 2013), it does not involve tectonic regularization, which results in smoother transitions. We chose the lithosphere-asthenosphere boundary (LAB) from the LithoRef18 model (Afonso et al., 2019), calculated by joint inversion and analysis of multiple data sets: gravity anomalies, geoid, satellite-derived gravity gradients, and elevation along with seismic, thermal, and petrological prior information. The initial lithospheric thickness is a hybrid model based on several global tomography models.

Along with depth information, we also used several distance measures to geological features like trenches, transform faults, and ridges from the PLATES project by Coffin et al. (1997). Likewise, we included the distance to young rifts from Şengör and Natal'in (2001), where young means not older than 65 Ma (according to Goutorbe et al. (2011)). Elevated heat flow is closely related to the vicinity of volcanoes. Geothermal exploration is often carried out in volcanically active regions, which might introduce a bias. On the other hand, volcanoes can be useful indicators of high heat flow. We used locations of Pleistocene volcanoes from the Global Volcanism Program (2013). For Antarctica, possible locations are given by van Wyk de Vries et al. (2018), who used ice sheet bed-elevation data to locate conical structures in West Antarctica, supported by aerogravity, satellite imagery, and databases of confirmed volcanoes. Yet, we only took results with an intermediate or higher certainty factor (≥3).

Indicators of the geological composition of the crust are gravity anomalies. We used the mean curvature, inferred from the two horizontal and independent satellite gravity gradient components (Ebbing et al., 2018). This parameter is used to interpret gravity anomalies by trying to delineate geometric information of subsurface structures from an observed nongeometric quantity. It describes how much a line deviates from being straight or a surface from being flat. Also, we wanted to reduce the effect from the density contrast between crust and mantle since we are already employing a Moho depth individually and, therefore, used the isostatic residuals.

We, furthermore, used a composed topography with the global EARTH2014 (Hirt & Rexer, 2015) and the Antarctic Bedmachine model (Morlighem et al., 2020). The former is an improved global topographic model compared to ETOPO1 (Amante & Eakins, 2009), which we combined with the newest available topographic high-resolution model of Antarctica based on mass conservation.

Schaeffer and Lebedev (2015) produced a tectonic regularization of the Earth's crust by clustering the resulting large phase and group velocity data set from the global tomographic model SL2013sv (Schaeffer & Lebedev, 2013). It clusters six continental and oceanic regions of different ages with a relatively low resolution of two degrees. To handle this categorical feature, we label encoded the clusters in the order of decreasing age: cratons: 1, PreC, fold belts modified cratons: 2, Phanerozoic continents: 3, Rigdes Backarcs: 4. We decided not to one-hot encode this feature to decrease the dimensionality and facilitate the interpretation. Nevertheless, training the model with the one-hot encoded tectonic feature leads to almost identical results.

The magnetic signal from the crust is an important feature that potentially correlates strongly with GHF. The deepest magnetic sources can be assumed to correlate to the Curie depth, the temperature at which rocks (mostly magnetite for the crust) lose their ability to orientate in the direction of the applied field. The depth of this isotherm would be one of the most important factors for estimating GHF when known with low uncertainty (Lösing et al., 2020). We did not use Curie depth estimates themselves because it was always by far the most dominant feature in first tests. Regarding the uncertainties behind the Curie depth estimation (Núñez Demarco et al., 2020; Pappa & Ebbing, 2021), we prefer an independent prediction. Therefore, we use magnetic data from the satellite magnetic lithosphere model LCS-1 (Olsen et al., 2017). One problem arising with magnetic data is the directional dependency of the crustal field. To circumvent this, we use the magnetic field anomalies after reduction to the pole with an equivalent dipole approach (Ebbing et al., 2021).

In addition, we use the vertically integrated susceptibility model by Hemant and Maus (2005). The VIS model is established with a GIS-approach using a global geological map as a base. Within the geological units, laboratory susceptibility of different rock types and seismically inferred crustal thickness is used to define an optimized model by inverting satellite magnetic data. Although the model is not entirely independent from the magnetic data sets, we use it as an indicator of the prevailing geology and trust that the machine learning approach will be able to make an adequate weighting of the individual data sets.

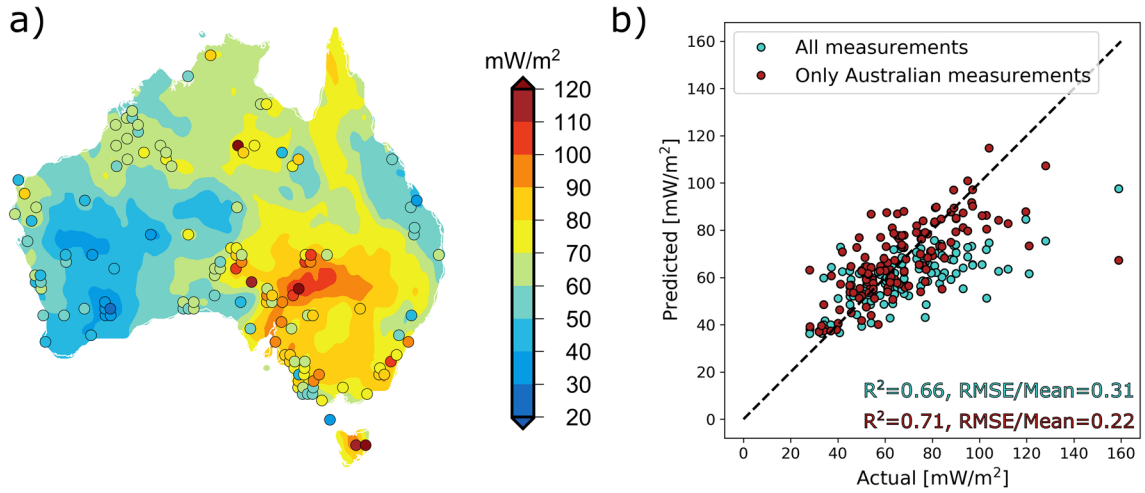

Figure 1. (a) Predicted heat flow for Australia with exclusively Australian measurements. All features from Table 1 with the regional Moho and LAB depth models are used. Actual measurements are marked as circles. (b) Comparison between actual measurements and predicted values in Australia. Predictions that include all global measurements in the training set are shown in light blue and including only Australian measurements in dark red. LAB, lithosphere-asthenosphere boundary.

3.3. Regional Data for Antarctica and Its Gondwana Neighbours

Besides the global data sets, we add regional data sets to the analysis. While our focus is on an improved assessment of GHF in Antarctica, we will also replace the Moho depth from the global data sets for the adjacent continents. Latest during Gondwana, southern Africa, Australia, and East Antarctica were connected (Meert & Van Der Voo, 1997). Tectonic affiliations can be observed (Daczko et al., 2018; Mulder et al., 2019) and are supported by gravity and magnetic data (Aitken et al., 2016; Ebbing et al., 2021; Ferraccioli et al., 2011). Similar to Pollett et al. (2019), we assume here that the tectonic history of these now separated continents has been relatively quiescent and that the crustal part is primarily influencing the surface heat flow in thermotectonic stable terrains (Förster & Förster, 2000; Mareschal & Jaupart, 2013).

Regional data for this part of Gondwana might improve the prediction model. The data coverage and quality for Australia are significantly better than for the other parts, and hence, we use Australia for the first test of our approach. For Australia, an estimate of the Moho depth is available by AuSREM (Australian Seismological Reference Model) (Kennett et al., 2018). For Southern Africa, we use the seismic Moho depth model by Youssof et al. (2013), which is concentrated on the Kalahari craton and not the entire region. The lithospheric model for Antarctica is based on the integrated geophysical data from Pappa et al. (2019). Additionally, we evaluate the application of a seismological model AN1 by An et al. (2015a, 2015b). The latter is modified so that the West Antarctic Moho (everything west of the Transantarctic Mountains) of AN1 is replaced with the most recent and refined model by Shen et al. (2018) (called Shen18, hereafter).

4. Results

First, the validity of the machine learning approach is tested for Australia. Following, we investigate the significance of individual features and their influence on the model statistics. Next, we show the predicted geothermal heat flow in Antarctica and finally present some of the uncertainties of this approach.

4.1. Predicting Heat Flow for a Well-Known Region

For the first test of our approach, we predict GHF for Australia, where considerably more measurements are available (values have been prepared as described in Section 3.1) and geophysical information might be more accurate than for Antarctica. Figure 1a shows the prediction for the Australian continent and the available measurements. The model agrees well with most of the measurements, but few very high values (≥120 mW/m^2) are somewhat underestimated. However, the result resembles the kriging model from Pollett

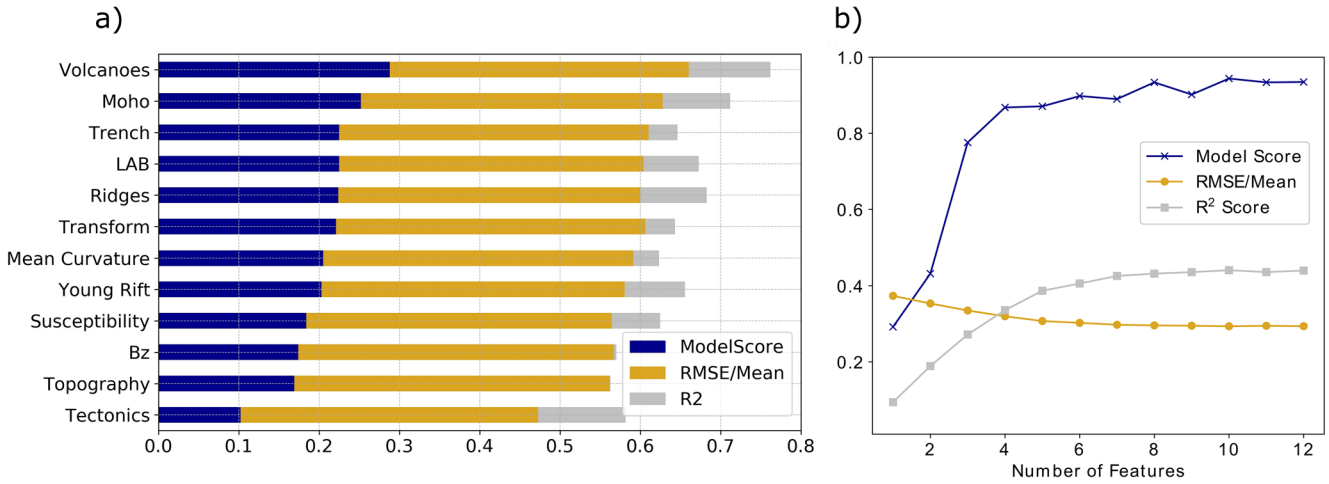

Figure 2. (a) Attained model and R^2 scores and normalized RMSE of every individual feature sorted by model score (LAB: lithosphere-asthenosphere boundary, Bz: vertical magnetic component). (b) Scores and error progression with increasing number of features used in the algorithm. Starting with distance to volcanoes and proceeding with features with next highest model score. RMSE, root-mean-square error.

et al. (2019) with the three major provinces: eastern, central, and western Australia, ranging from values between ~30 and 40 mW/m^2 in the Yilgarn Craton to 100–120 mW/m^2 in the Cenozoic part of East Australia and the Adelaide Fold Belt.

Because of the relatively high amount of measurements, we can use them exclusively to establish the Australian model. This leads to a measurably better correlation (R^2 increases by 0.05) between actual and predicted values for Australia than by using all global values (Figure 1b). Only one value of 159 mW/m^2 stands out. It is more accurately predicted by all global measurements, due to the higher amount of high heat flow values (≥160 mW/m^2) within the global data. For Antarctica, this approach is not practicable because of the sparsity of continental measurements.

4.2. Testing Individual Features

The prediction strongly relies on the deployed features. Therefore, it is important to review their quality and their significance for heat flow. We can evaluate the different impacts of each feature on the training set (model score), the test set (R^2 score), and the normalized RMSE by running the algorithm with only one feature at a time (Figure 2). It is noticeable that high model scores are not necessarily accompanied by high R^2 scores or the other way around. The scores range from 0.10 to 0.29 for the training set and from 0.001 to 0.11 for the test set. However, the RMSE does not vary significantly, with values between 0.37 and 0.39. The distance to volcanoes is yielding the highest score in the model training and the second-lowest RMSE. Hence, the proximity to volcanic regions is essential for heat flow prediction and is most accurate according to the regression boosting algorithm. The feature "Tectonics" inferred from seismic tomography indicates a high R^2 score but a low model score.

Further, we investigated the influence of the number of features by gradually increasing it from 1 to 12 (only one Moho and LAB depth, Figure 2). We successively add the feature with the next highest model score, according to their ranking. Therefore, we start with the distance to volcanoes, add Moho depth subsequently, and so on. The progressions of the model score and R^2 score and the normalized RMSE show convergent behavior. Up to six features, the scores and the RMSE change noticeably, after which they reach a plateau, and adding more features has no influence on these measures anymore. The resulting scores for all 12 features are 0.94 for the training set and 0.44 for the test set, meaning that our prediction model explains almost half of the data variety. The normalized RMSE settles in a value of 0.29, so on average, the prediction makes a relative error of 29%.

4.3. Heat Flow Prediction for Antarctica

The 12 different features (Table 1) are now used to predict the heat flow for Antarctica. For the Antarctic Moho and LAB depths, like in all former calculations, we chose the lithospheric model by Pappa et al. (2019). Figure 3 shows the resulting heat flow model and the few existing measurements on the continent with their respective measured heat flow value.

Overall, the machine learning approach predicts higher heat flow in West than in East Antarctica, which is consistent with previous heat flow models (e.g., An et al., 2015b; Martos et al., 2017; Shen et al., 2020). The predicted mean heat flow of 63 mW/m^2 is close to the global mean of 64 mW/m^2. Exceptionally high values up to 156 mW/m^2 are predicted for the region between Ellsworth Land and Marie Byrd Land, which are lower than the extremely high measurement of 180 mW/m^2 (Fisher et al., 2015) in this area. The heat flow in East Antarctica appears to be more homogeneous and ranges mostly between 50 and 60 mW/m^2. However, we find the lowest values (<40 mW/m^2) in Dronning Maud Land and around Dome Fuji.

Most of the available measurements in Antarctica fit well to the predictions. In general, they are somewhat underestimated. Plotting predicted values against their actual counterparts (Figure 4) shows that most predictions are close to the exact prediction on the diagonal line. Still, heat flow values higher than 90 mW/m^2 are all below. Especially, the exceptionally high value of 187 mW/m^2 in Enderby Land, which is the binned mean of two measurements (Nagao & Kaminuma, 1983) is immensely underpredicted. It is visible that this particular value has no considerable influence on the prediction and the immediate neighbor, a relatively low measurement of 50 mW/m^2 is fitted better. In contrast, the high value beneath the West Antarctic Ice Sheet has a significant influence, and a large area exhibits noticeably warm heat flow.

How the features contributed to the minimization of the loss function can be shown as importance of each feature. According to the algorithm, proximity to volcanoes and Moho depth have the most substantial effect on heat flow predictions (Figure 4). The subsequent order of feature importance's can vary slightly. Magnetic field and LAB seem to have an inferior influence and are, in this case, the two least important features.

4.4. Uncertainties

The uncertainties of this method are considered to be significantly dependent on the features used. Figure 5 shows heat flow predictions for three different selections of features and their respective differences to the result presented above (Figure 3).

Because of the high importance of the Moho depth on the prediction (Figure 4), we investigate the influence of using a different lithospheric model than in Section 4.3. Therefore, we exchange it with the combined lithospheric model AN1 and Shen18. The prediction for this case shows mainly colder values, especially in East Antarctica (Figures 5a and 5b). In a broad region of George V Land and Wilkes Basin, we can observe the highest differences of about 30 mW/m^2.

Further, we show the heat flow prediction with only global input features (Figures 5c and 5d). It is visible that coastal regions are slightly colder, and central Antarctica exhibits slightly warmer areas.

Lastly, we used only six features with the highest model scores according to Figure 2 (volcanoes, Moho depth, trenches, LAB, ridges, and transform faults). Here, the same regional models as in Section 4.3 are used. Compared to the results in Section 4.3, both East and West Antarctica are considerably colder, particularly between Ellsworth Land and Marie Byrd Land with the highest differences up to 66 mW/m^2 (Figures 5e and 5f).

We calculated the maximum absolute difference between all presented prediction models (results from Section 4.3 and Figures 6a–6e). It is visible that West Antarctica is considerably more uncertain than East Antarctica, with absolute differences of up to about 82 mW/m^2. High uncertainties are also observed in George V Land and Terre Adélie, whereas most of East Antarctica indicates minor differences between 0 and 25 mW/m^2. The resulting maximum and minimum heat flow maps are intended to indicate the upper and lower boundary for potential dynamic ice sheet simulations (Figure 6).

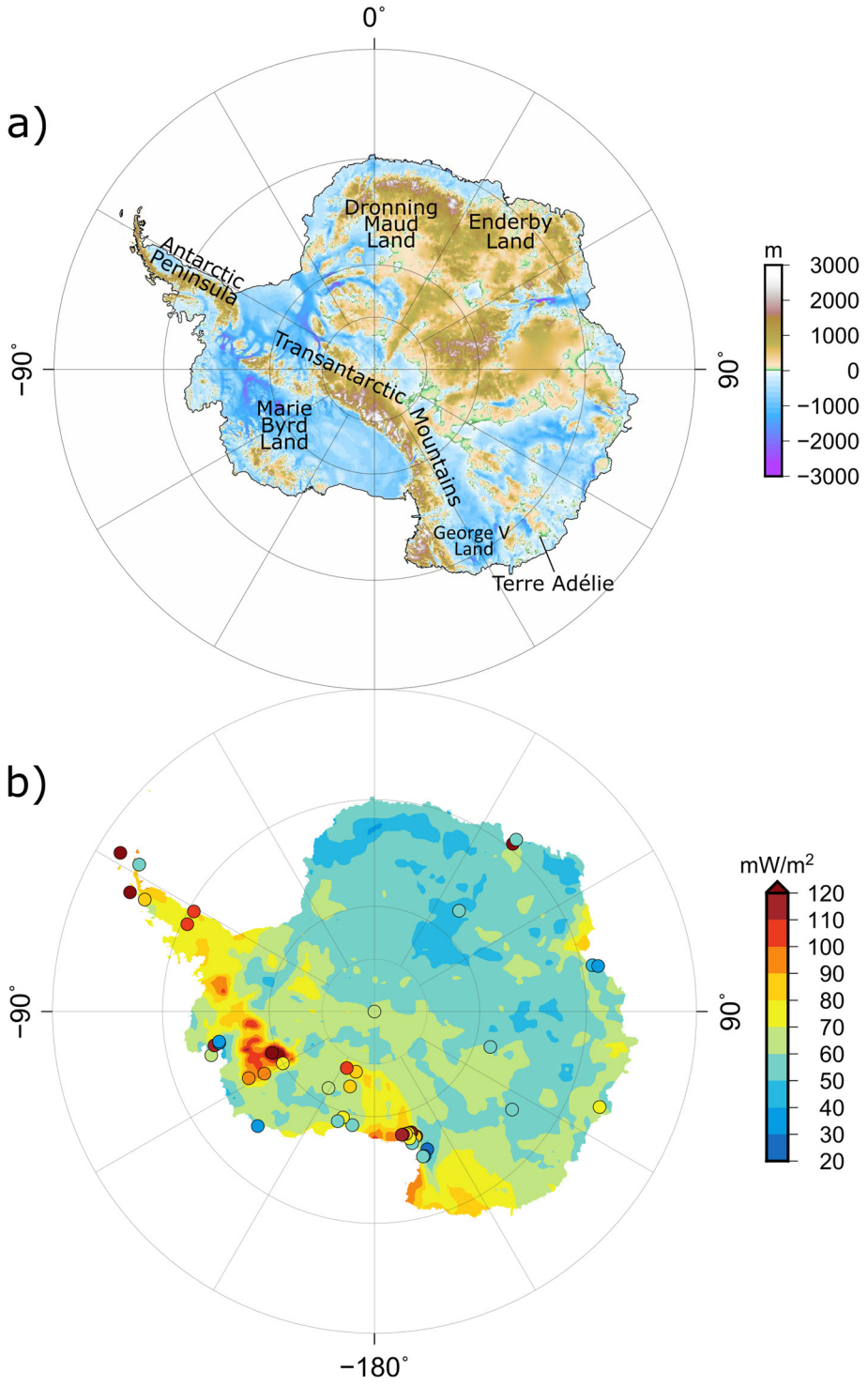

Figure 3. (a) Bedrock topography by Morlighem et al. (2020) and indications of Antarctic regions. (b) Predicted heat flow with regional Moho and LAB depth models for Antarctica, Australia, and South Africa. With Antarctic lithospheric depth models by Pappa et al. (2019). The actual measurements are marked as circles. LAB: lithosphere-asthenosphere boundary.

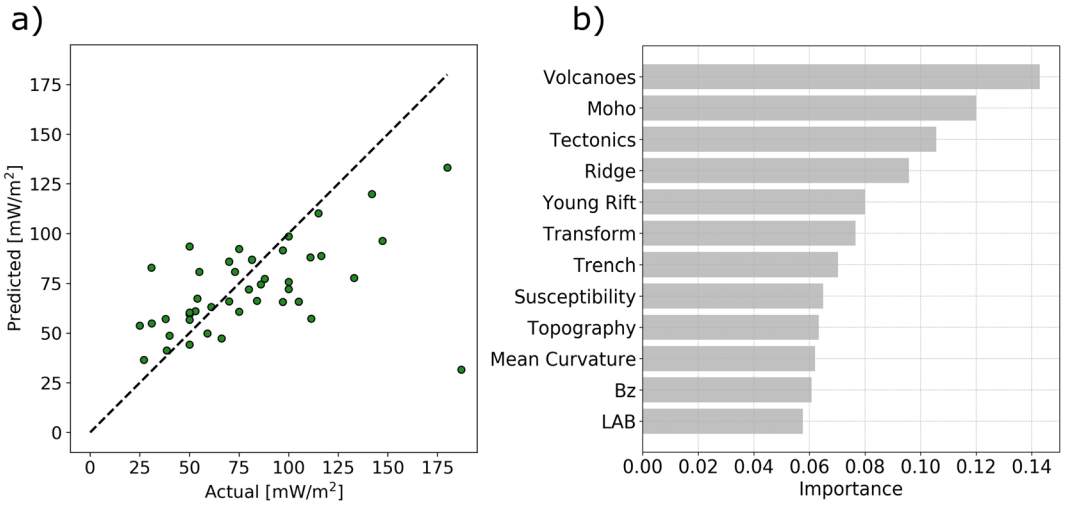

Figure 4. (a) Fit between actual and predicted heat flow in Antarctica. (b) Relative importances (see Section 2.2) of the individual features on the trained prediction model. Bz: vertical magnetic component, LAB: lithosphere-asthenosphere boundary. The sum of the relative importances is 1.

5. Discussion

The established prediction model exhibits an R^2 score of 0.44 in the test set and a relative RMSE of 29%. Both values are lower than the respective results from Rezvanbehbahani et al. (2017), which most probably results from the applied Gauss filter on heat flow in their study. The reduced variability of the heat flow values can be captured more accurately by the low-resolution global models. We decided not to Gauss filter the measurements because binning and excluding extremely high values (>200 mW/m^2) is already a significant modification.

The first test for Australia shows a close fit between actual and predicted heat flow. The actual measured values are considered to be more reliable and to better reflect the regional scale due to the higher spatial coverage. Further, Australian heat flow estimates are derived from bedrock boreholes in contrast to most Antarctic ones, which allows the measurement of thermal conductivity and heat production from samples (e.g., Mather et al., 2018; Pollett et al., 2019). Thus, regarding the close fit and the agreement with previous studies (Artemieva & Mooney, 2001; Cull, 1982; Pollett et al., 2019), we are optimistic that the method gives reasonable results.

Likewise, for Antarctica, the predicted values fit closely to the actual measurements. However, values higher than 90 mW/m^2 are predicted slightly colder. One reason for this is possibly that the ratio between global heat flow measurements above and below 90 mW/m^2 is about 1:3 and for continental values almost 1:4. On the other hand, measurements are likely biased toward tectonically active regions and hence high values due to the nature of geothermal exploration. Therefore, we are not aiming for a perfect prediction of the measurements because that would mean overfitting, which is already restrained by the algorithm. And, regarding the uncertainties that go along with these measurements (Burton-Johnson et al., 2020), it is probably more realistic to have low variance and hence a more reasonable regional trend.

On the other hand, the method primarily relies on the measurements. As a result, the area around the South Pole is likely to exhibit a close fit to the value of 61 $\pm$ 1 mW/m^2 (Price et al., 2002), which is different from suggested elevated heat flow in this area based on estimated melt rates from ice sheet modeling (Jordan et al., 2018).

Different high measurements have distinct influences on the predicted heat flow. At the West Antarctic Ice Sheet (WAIS) Divide (Lon: −112.1, Lat: −79.5), there are two relatively high measurements of 180 $\pm$ 40 mW/m^2 (Fisher et al., 2015) and 240 mW/m^2 (Clow et al., 2012), where latter has been filtered out before binning. Both go along with very high uncertainties (the former value is calculated from an earlier study on ice cores by Fudge et al. (2013) so no thermal equilibration was accomplished). Though there are two of these high

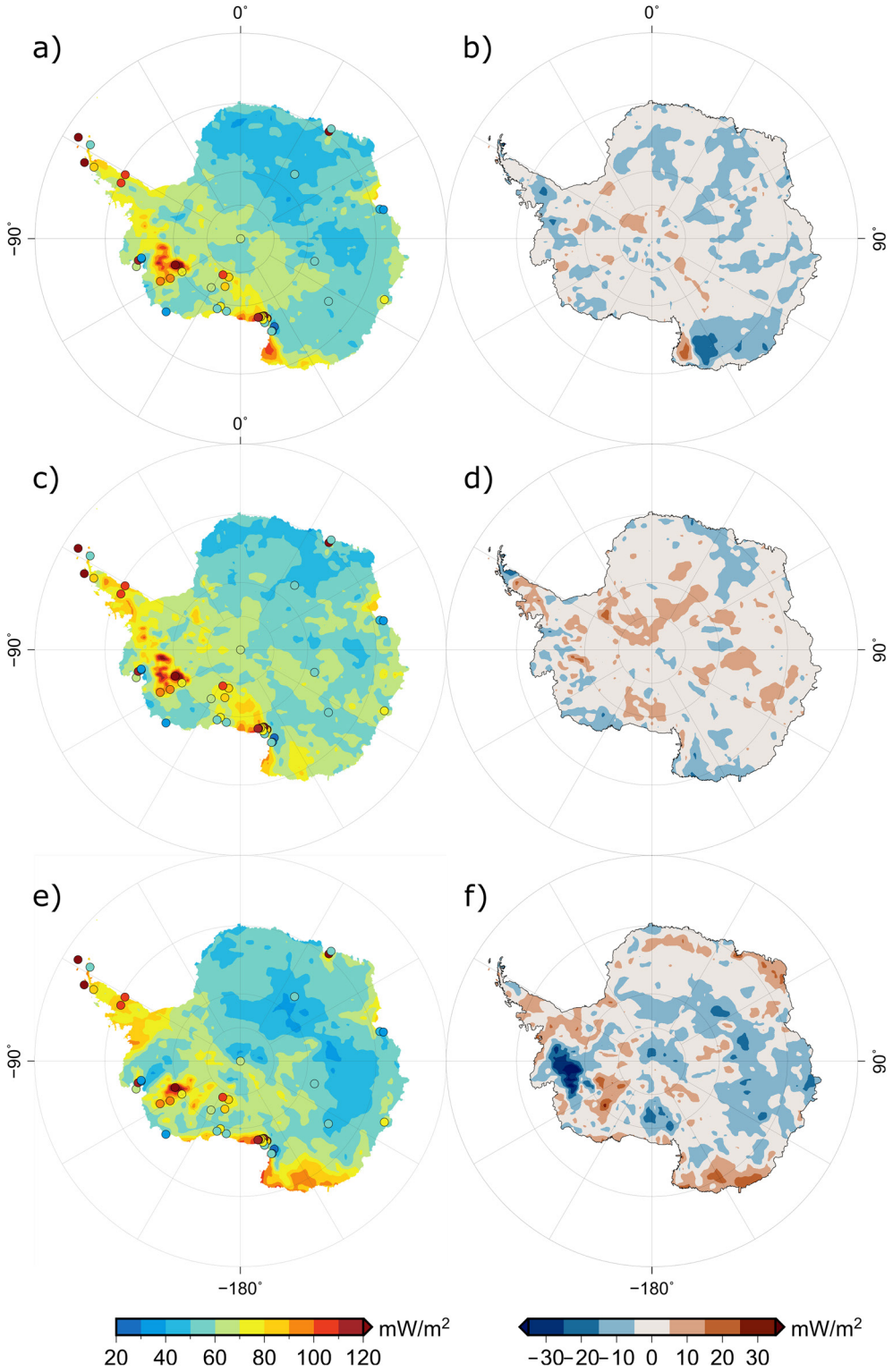

Figure 5. Predicted heat flow models for different feature selections (a, c, and e) and the respective differences to the result from Section 4.3 (b, d, and f, the model from the previous section is subtracted from the respective heat flow models in this section). (a + b) A different lithospheric model (combination of AN1 and Shen18, see Section 3). (c + d) Only global models. (e + f) Only six features with the highest model scores according to Figure 2 (volcanoes, Moho, trenches, LAB, ridges, and transform). Actual measurements are marked as circles. LAB: lithosphere-asthenosphere boundary.

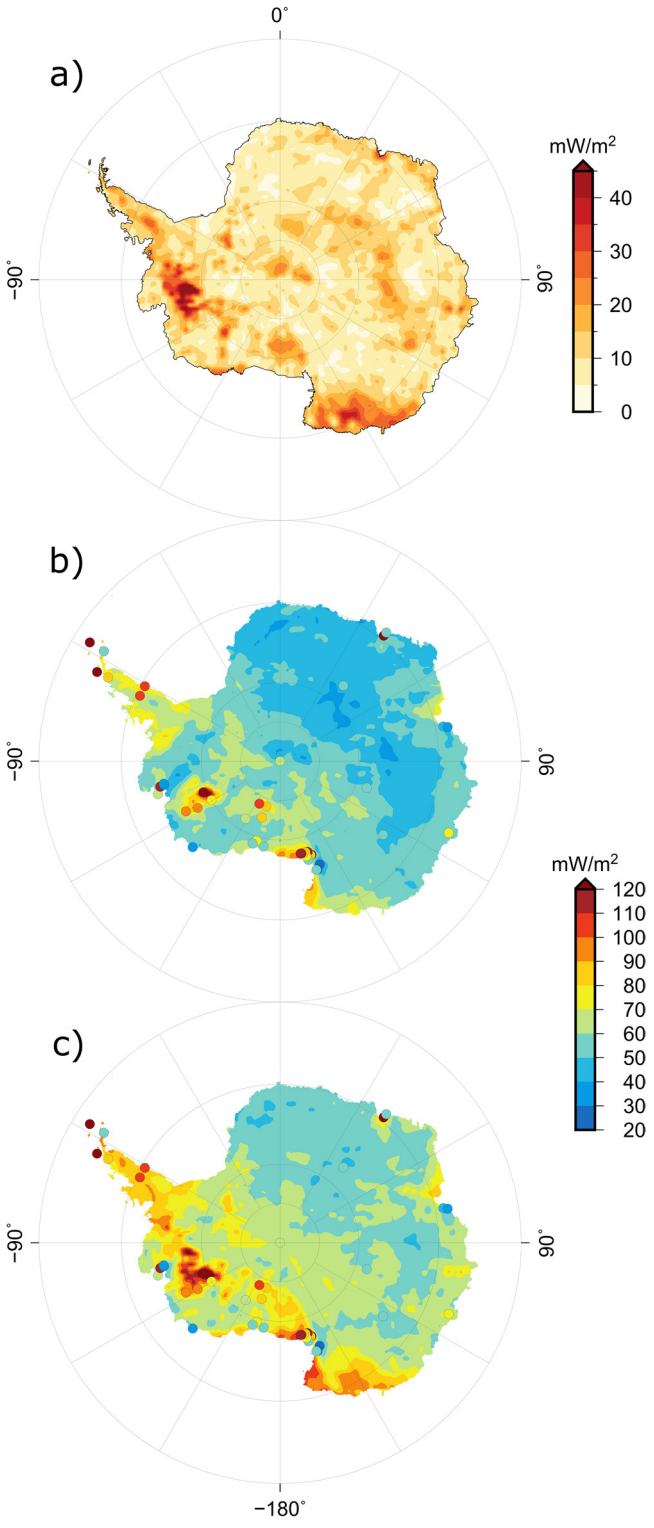

Figure 6. (a) Maximum absolute difference between all predicted heat flow models from Sections 4.3 and 4.4. (b) Resulting minimum heat flow. (c) Resulting maximum heat flow. Actual measurements are marked as circles.

measurements in the same place from different studies, it is more likely to have elevated heat flow in this area. In this study, we show the results with the inclusion of the former value into the training set. This yields noticeably high heat flow in West Antarctica, yet not as high as the actual measurements. Omitting this value leads to significantly colder heat flow in this area, indicating that the geological setting might be unique. One high value in East Antarctica (Lon: −39.5, Lat: −69.5) results from binning two values 184 and 190 mW/m^2 from one publication (Nagao & Kaminuma, 1983). Again both of these values are highly uncertain. A very close value of 50 mW/m^2, also from the same publication, probably compensates for their influence (all three values are within ∼30 km). A comparably high variability is also found, for example, by (Begeman et al., 2017) measuring a value of 88 ± 7 mW/m^2 near the Whillans ice stream and close (∼100 km) to another measurement of 285 ± 80 mW/m^2 (Fisher et al., 2015). They suggest shallow magmatic intrusions or fluid advection in the crust as a possible explanation. In our model, we did not account for such high variability.

Testing the inclusion of global heat flow measurements up to 400 mW/m^2 in the algorithm leads to slightly increased heat flow in already warm regions with differences up to 40 mW/m^2 (Figure S4). Still, values over 90 mW/m^2 are underpredicted (Figure S5).

In this study, we focused on a feasible selection of features and analyzed their influence on the prediction. Using data, which are not available in polar regions due to the thick ice layer like heat production provinces or rock type, might improve the statistics for global prediction but has no added value for Antarctic heat flow prediction. Distinct choices of features can lead to very different predictions, especially for regions without constraining measurements, even if the model statistics do not change.

According to the algorithm, proximity to the next closest volcano and crustal thickness are good predictors with high training and test scores. Tectonic units by Schaeffer and Lebedev (2015) display contradicting scores, yielding the lowest model score but at the same time the highest R^2 score. This might emanate from its categorical character and the large-scale structures, which lead to a low variance prediction model. However, the order of feature importance for the final heat flow prediction (Figure 4) does not necessarily coincide with the order of the individual scores (Figure 2), which indicates that the algorithm builds a more complex relationship among the features than a linear regression would probably do.

Global models are often strongly inaccurate in Antarctica due to low data coverage. Therefore, we decided to included regional data and models, which are more detailed and incorporate more information from, for example, satellite data or exclusive Antarctic surveys. For the final heat flow model, we preferred the lithospheric model by Pappa et al. (2019) because it combines satellite gravity gradients with seismological estimates (from AN1), thermodynamic modeling, and the consideration of isostasy. Subsequently, it is validated with seismic Moho depth estimates. The combination of different geophysical observables makes the model more robust. The alternative lithospheric model (combination of AN1 and Shen18) exhibits lower values in George V Land and Terre Adélie. Specifically, this area represents the Antarctic tectonic counterpart of the Australian Gawler Craton (Payne et al., 2009; Williams et al., 2018). The

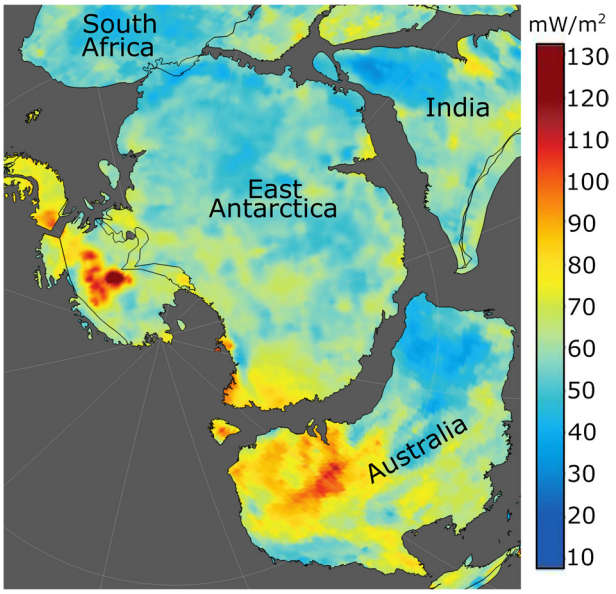

Figure 7. Heat flow prediction in the Gondwana framework. Results are visualized with the software GPlates (Mueller et al., 2018) and a rotation age of 200 Ma from the plate motion model by Mueller et al. (2019). For Antarctica, we used the results from Section 4.3 and for Australia from Section 4.1.

high heat flow region in southeast Australia fits well to the warm region in George V Land in our presented map (Section 4.3), which supports our decision. At all conjugate margins, the predicted heat flow in East Antarctica (Section 4.3) exhibits visible connections to its presumed tectonic counterparts (Figure 7). In contrast, previous heat flow models (An et al., 2015b; Martos et al., 2017; Shen et al., 2020) do not indicate these connections (Pollett et al., 2019).

However, apart from the east-west division, there is no noticeable consensus. While the magnetic model by Martos et al. (2017) exhibits very high heat flow regions (130–180 mW/m^2) in West Antarctica, the model by Shen et al. (2020) is relatively cold and no heat flow higher than 90 mW/m^2 is found. Our result could be classified as an intermediate model with values between these rather extreme models. For comparison, we calculated the maximum absolute difference between the models by Martos et al. (2017) and Shen et al. (2020) and the predicted final model from this study (Figure 8). Therefore, we resampled the former models to a resolution of 0.5°. We can observe that the heat flow models mainly agree in central East Antarctica and very poorly in West Antarctica with a maximum absolute difference of 125 mW/m^2.

6. Conclusions

Machine learning based on gradient boosting regression is a suitable approach for predicting heat flow, which has been demonstrated for Australia and the largely unknown content of Antarctica. The machine learning approach overcomes simplifications like using laterally constant thermal values and does not rely on a single geophysical method but uses several different features. Further, the algorithm learns from other continents with higher coverage of geophysical data and available heat flow measurements.

Our new Antarctic GHF model incorporates all available measurements and considers the information of in total 12 geological and geophysical observables, which contain information on regional tectonic settings and geology. To study the advantage of using regional data sets, we included crustal depth models of Antarctica and its conjugate margins of South Africa and Australia to improve and specify the prediction

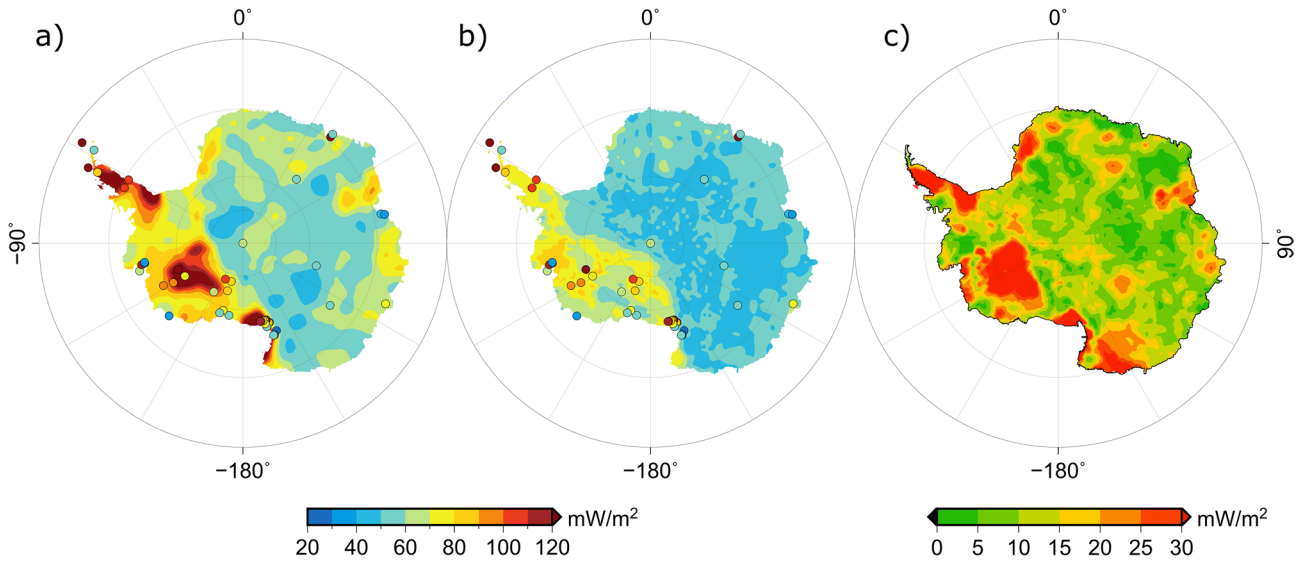

Figure 8. Published heat flow models by (a) Martos et al. (2017) and (b) Shen et al. (2020). Actual measurements are marked as circles. (c) Agreement between both models and the result of this study (Section 4.3) indicated by the maximum absolute differences.

for Antarctica. A simple Gondwana reconstruction shows the similarities in heat flow predictions for the conjugate margins, illustrating the added value using the formerly adjacent continents as guidance for East Antarctica. While uncertainties remain, we provide minimum and maximum results, which can be used as input for further sensitivity analysis, for example, for ice sheet dynamics and ice flow (e.g., Rogozhina et al., 2012; Seroussi et al., 2017). Future efforts should not only aim to improve the statistics of the prediction model but deliberate about which and how many features are reasonable and trustworthy. As shown here, the addition of regional data is preferred for global data with limited accuracy in polar regions.

Furthermore, parameters like heat production and thermal conductivity have not yet been considered but would certainly change the results significantly (Lösing et al., 2020). However, to achieve this, a wide rock property database must be established. Also, using updated data like a new tomography for cluster analysis of tectonic units along with a multivariate analysis of lithospheric domain boundaries like Stål et al. (2019) could be beneficial.

Acronyms: GHF, Geothermal Heat Flow; AN1, Lithospheric model consisting of Moho and lithosphere-asthenosphere boundary depths by An et al. (2015a, 2015b); Shen18, Moho depth model by Shen et al. (2018).

Data Availability Statement

The authors are grateful for the revision and comments from Wolfgang Szwillus and thank Jonas Liebsch for the compilation of both global heat flow data sets. Heat flow data bases used in this study: (a) Hasterok (2019) http://www.heatflow.org/ (downloaded 10.02.2020, an updated version is now available by Jennings et al. (2021)). (b) Lucazeau (2019) https://doi.org/10.1029/2019GC008389 (downloaded 10.02.2020). (c) Burton-Johnson et al. (2020) https://github.com/RicardaDziadek/Antarctic-GHF-DB (downloaded 19.08.2020). XGBoost library is available here: https://github.com/tqchen/xgboost. GPlates open-source software: https://www.gplates.org/. Data and code used in this study are available here: https://doi.org/10.5281/zenodo.4311273.

Acknowledgments
We thank the editor and two anonymous reviewers for their constructive criticism that helped to improve our manuscript. This work was supported by the Deutsche Forschungsgemeinschaft (DFG) in the framework of the priority programme "Antarctic Research with comparative investigations in Arctic ice areas" SPP 1158 by a grant (Grant No. EB 255/8-1). Open access funding enabled and organized by Projekt DEAL.

References

Afonso, J. C., Salajegheh, F., Szwillus, W., Ebbing, J., & Gaina, C. (2019). A global reference model of the lithosphere and upper mantle from joint inversion and analysis of multiple data sets. *Geophysical Journal International*, *217*(3), 1602–1628. https://doi.org/10.1093/gji/ggz094

Aitken, A., Betts, P., Young, D., Blankenship, D., Roberts, J., & Siegert, M. (2016). The Australo-Antarctic Columbia to Gondwana transition. *Gondwana Research*, *29*(1), 136–152. https://doi.org/10.1016/j.gr.2014.10.019

Amante, C., & Eakins, B. W. (2009). *ETOPO1 arc-minute global relief model: Procedures, data sources and analysis.*

An, M., Wiens, D. A., Zhao, Y., Feng, M., Nyblade, A. A., Kanao, M., et al. (2015a). S-velocity model and inferred Moho topography beneath the Antarctic plate from Rayleigh waves. *Journal of Geophysical Research: Solid Earth*, *120*, 359–383. https://doi.org/10.1002/2014JB011332

An, M., Wiens, D. A., Zhao, Y., Feng, M., Nyblade, A. A., Kanao, M., et al. (2015b). Temperature, lithosphere-asthenosphere boundary, and heat flux beneath the Antarctic plate inferred from seismic velocities. *Journal of Geophysical Research: Solid Earth*, *120*, 8720–8742. https://doi.org/10.1002/2015JB011917

Artemieva, I. M., & Mooney, W. D. (2001). Thermal thickness and evolution of precambrian lithosphere: A global study. *Journal of Geophysical Research*, *106*(B8), 16387–16414. https://doi.org/10.1029/2000JB900439

Bachu, S. (1988). Analysis of heat transfer processes and geothermal pattern in the Alberta Basin, Canada. *Journal of Geophysical Research*, *93*(B7), 7767–7781. https://doi.org/10.1029/JB093iB07p07767

Begeman, C. B., Tulaczyk, S. M., & Fisher, A. T. (2017). Spatially variable geothermal heat flux in West Antarctica: Evidence and implications. *Geophysical Research Letters*, *44*, 9823–9832. https://doi.org/10.1002/2017GL075579

Burton-Johnson, A., Dziadek, R., & Martin, C. (2020). Geothermal heat flow in Antarctica: Current and future directions. *The Cryosphere Discussions*, 1–45. https://doi.org/10.5194/tc-2020-59

Chen, T., & Guestrin, C. (2016). XGBoost: A scalable tree boosting system. In *Proceedings of the 22nd ACM SIGKDD International Conference on Knowledge Discovery and Data Mining*. https://doi.org/10.1145/2939672.2939785

Clow, G., Cuffey, K., & Waddington, E. (2012). High heat-flow beneath the central portion of the West Antarctic Ice Sheet. *AGU Fall Meeting Abstracts* (Vol. 2012, pp. C31A-0577).

Coffin, M. F., Gahagan, L. M., & Lawver, L. A. (1997). *Present-day plate boundary digital data compilation* (Technical Report). Institute for Geophysics.

Cull, J. (1982). An appraisal of Australian heatflow data. *BMR (Bureau of Mineral Resources) Journal of Australian Geology and Geophysics*, *7*, 11–21.

Daczko, N. R., Halpin, J. A., Fitzsimons, I. C. W., & Whittaker, J. M. (2018). A cryptic Gondwana-forming orogen located in Antarctica. *Scientific Reports*, *8*, 8371. https://doi.org/10.1038/s41598-018-26530-1

Ebbing, J., Dilixiati, Y., Haas, P., Ferraccioli, F., & Scheiber-Enslin, S. (2021). East Antarctica magnetically linked to its ancient neighbours in Gondwana. *Scientific Reports*, *11*, 5513. https://doi.org/10.1038/s41598-021-84834-1

Ebbing, J., Haas, P., Ferraccioli, F., Pappa, F., Szwillus, W., & Bouman, J. (2018). Earth tectonics as seen by GOCE-enhanced satellite gravity gradient imaging. *Scientific Reports*, *8*, 16356. https://doi.org/10.1038/s41598-018-34733-9

Ferraccioli, F., Finn, C. A., Jordan, T. A., Bell, R. E., Anderson, L. M., & Damaske, D. (2011). East Antarctic rifting triggers uplift of the Gamburtsev Mountains. *Nature*, *479*(7373), 388–392. https://doi.org/10.1038/nature10566

Fisher, A. T., Mankoff, K. D., Tulaczyk, S. M., Tyler, S. W., Foley, N., & WISSARD Science Team. (2015). High geothermal heat flux measured below the West Antarctic Ice Sheet. *Science Advances*, *1*(6), e1500093. https://doi.org/10.1126/sciadv.1500093

Förster, A., & Förster, H.-J. (2000). Crustal composition and mantle heat flow: Implications from surface heat flow and radiogenic heat production in the Variscan Erzgebirge (Germany). *Journal of Geophysical Research*, *105*(B12), 27917–27938. https://doi.org/10.1029/2000JB900279

Friedman, J. H. (2001). Greedy function approximation: A gradient boosting machine. *Annals of Statistics*, *29*(5), 1189–1232.

Fudge, T., Steig, E. J., Markle, B. R., Schoenemann, S. W., Ding, Q., Taylor, K. C., et al. (2013). Onset of deglacial warming in West Antarctica driven by local orbital forcing. *Nature*, *500*(7463), 440–444. https://doi.org/10.1038/nature12376

Global Volcanism Program. (2013). *Volcanoes of the world, v. 4.9.0 (04 June 2020)*. Smithsonian Institution. https://doi.org/10.5479/si.GVP.VOTW4-2013

Goutorbe, B., Poort, J., Lucazeau, F., & Raillard, S. (2011). Global heat flow trends resolved from multiple geological and geophysical proxies. *Geophysical Journal International*, *187*(3), 1405–1419. https://doi.org/10.1111/j.1365-246x.2011.05228.x

Hasterok, D. (2019). *Website*. Retrieved from http://www.heatflow.org

Hemant, K., & Maus, S. (2005). Geological modeling of the new champ magnetic anomaly maps using a geographical information system technique. *Journal of Geophysical Research*, *110*, B12103. https://doi.org/10.1029/2005JB003837

Hirt, C., & Rexer, M. (2015). Earth2014: 1 arc-min shape, topography, bedrock and ice-sheet models—Available as gridded data and degree-10,800 spherical harmonics. *International Journal of Applied Earth Observation and Geoinformation*, *39*, 103–112. https://doi.org/10.1016/j.jag.2015.03.001

Jennings, S. S., Hasterok, D., & Lucazeau, F. (2021). Thermoglobe: Extending the global heat flow database. *Journal TBD*.

Jordan, T. A., Martin, C., Ferraccioli, F., Matsuoka, K., Corr, H., Forsberg, R., et al. (2018). Anomalously high geothermal flux near the south pole. *Scientific Reports*, *8*(1), 16785. https://doi.org/10.1038/s41598-018-35182-0

Kennett, B., Chopping, R., & Blewett, R. (2018). *The Australian continent: A geophysical synthesis*. ANU Press.

Larour, E., Morlighem, M., Seroussi, H., Schiermeier, J., & Rignot, E. (2012). Ice flow sensitivity to geothermal heat flux of pine island glacier, Antarctica. *Journal of Geophysical Research*, *117*, F04023. https://doi.org/10.1029/2012JF002371

Laske, G., Masters, G., Ma, Z., & Pasyanos, M. (2013). Update on CRUST1.0-A 1-degree global model of Earth's crust. *Geophysical Research Abstracts*, *15*, 2658.

Llubes, M., Lanseau, C., & Rémy, F. (2006). Relations between basal condition, subglacial hydrological networks and geothermal flux in Antarctica. *Earth and Planetary Science Letters*, *241*(3), 655–662. https://doi.org/10.1016/j.epsl.2005.10.040

Lösing, M., Ebbing, J., & Szwillus, W. (2020). Geothermal heat flux in Antarctica: Assessing models and observations by Bayesian inversion. *Frontiers in Earth Science*, *8*, 105. https://doi.org/10.3389/feart.2020.00105

Lucazeau, F. (2019). Analysis and mapping of an updated terrestrial heat flow data set. *Geochemistry, Geophysics, Geosystems*, *20*, 4001–4024. https://doi.org/10.1029/2019GC008389

Mareschal, J.-C., & Jaupart, C. (2013). Radiogenic heat production, thermal regime and evolution of continental crust. *Tectonophysics*, *609*, 524–534. https://doi.org/10.1016/j.tecto.2012.12.001

Martos, Y. M., Catalán, M., Jordan, T. A., Golynsky, A., Golynsky, D., Eagles, G., & Vaughan, D. G. (2017). Heat flux distribution of Antarctica unveiled. *Geophysical Research Letters*, *44*, 11417–11426. https://doi.org/10.1002/2017GL075609

Mather, B., McLaren, S., Taylor, D., Roy, S., & Moresi, L. (2018). Variations and controls on crustal thermal regimes in Southeastern Australia. *Tectonophysics*, *723*, 261–276. https://doi.org/10.1016/j.tecto.2017.12.015

Meert, J. G., & Van Der Voo, R. (1997). The assembly of Gondwana 800-550 Ma. *Journal of Geodynamics*, *23*(3), 223–235. https://doi.org/10.1016/S0264-3707(96)00046-4

Mooney, W. (2015). 1.11-Crust and lithospheric structure global crustal structure. In G. Schubert (Ed.), *Treatise on geophysics* (2nd ed., pp. 339–390). Oxford: Elsevier. https://doi.org/10.1016/B978-0-444-53802-4.00010-5

Morlighem, M., Rignot, E., Binder, T., Blankenship, D., Drews, R., Eagles, G., et al. (2020). Deep glacial troughs and stabilizing ridges unveiled beneath the margins of the Antarctic ice sheet. *Nature Geoscience*, *13*(2), 132–137. https://doi.org/10.1038/s41561-019-0510-8

Mueller, R. D., Cannon, J., Qin, X., Watson, R. J., Gurnis, M., Williams, S., et al. (2018). GPlates: Building a virtual earth through deep time. *Geochemistry, Geophysics, Geosystems*, *19*, 2243–2261. https://doi.org/10.1029/2018GC007584

Mueller, R. D., Zahirovic, S., Williams, S. E., Cannon, J., Seton, M., Bower, D. J., et al. (2019). A global plate model including lithospheric deformation along major rifts and orogens since the triassic. *Tectonics*, *38*, 1884–1907. https://doi.org/10.1029/2018TC005462

Mulder, J. A., Halpin, J. A., Daczko, N. R., Orth, K., Meffre, S., Thompson, J. M., & Morrissey, L. J. (2019). A multiproxy provenance approach to uncovering the assembly of East Gondwana in Antarctica. *Geology*, *47*(7), 645–649. https://doi.org/10.1130/G45952.1

Nagao, T., & Kaminuma, K. (1983). *Component parts of the world heat flow data collection [data set]*. PANGAEA. https://doi.org/10.1594/PANGAEA.808070

Núñez Demarco, P., Prezzi, C., & Sánchez Bettucci, L. (2020). Review of Curie point depth determination through different spectral methods applied to magnetic data. *Geophysical Journal International*, *224*(1), 17–39. https://doi.org/10.1093/gji/ggaa361

Olsen, N., Ravat, D., Finlay, C. C., & Kother, L. K. (2017). Lcs-1: A high-resolution global model of the lithospheric magnetic field derived from champ and swarm satellite observations. *Geophysical Journal International*, *211*(3), 1461–1477. https://doi.org/10.1093/gji/ggx381

Pappa, F., & Ebbing, J. (2021). Gravity, magnetics and geothermal heat flow of the Antarctic lithospheric crust and mantle (Vol. 56). London: Geological Society Memoirs. https://doi.org/10.1144/M56-2020-5

Pappa, F., Ebbing, J., Ferraccioli, F., & van der Wal, W. (2019). Modeling satellite gravity gradient data to derive density, temperature, and viscosity structure of the Antarctic lithosphere. *Journal of Geophysical Research: Solid Earth*, *124*, 12053–12076. https://doi.org/10.1029/2019JB017997

Payne, J. L., Hand, M., Barovich, K. M., Reid, A., & Evans, D. A. (2009). Correlations and reconstruction models for the 2500-1500 ma evolution of the Mawson Continent. *Geological Society, London, Special Publications*, *323*(1), 319–355. https://doi.org/10.1144/SP323.16

Pittard, M., Galton-Fenzi, B., Roberts, J., & Watson, C. (2016). Organization of ice flow by localized regions of elevated geothermal heat flux. *Geophysical Research Letters*, *43*, 3342–3350. https://doi.org/10.1002/2016GL068436

Pollett, A., Hasterok, D., Raimondo, T., Halpin, J. A., Hand, M., Bendall, B., & McLaren, S. (2019). Heat flow in southern Australia and connections with East Antarctica. *Geochemistry, Geophysics, Geosystems*, *20*, 5352–5370. https://doi.org/10.1029/2019GC008418

Price, P. B., Nagornov, O. V., Bay, R., Chirkin, D., He, Y., Miocinovic, P., et al. (2002). Temperature profile for glacial ice at the south pole: Implications for life in a nearby subglacial lake. *Proceedings of the National Academy of Sciences*, *99*(12), 7844–7847. https://doi.org/10.1073/pnas.082238999

Rezvanbehbahani, S., Stearns, L. A., Kadivar, A., Walker, J. D., & van der Veen, C. J. (2017). Predicting the geothermal heat flux in Greenland: A machine learning approach. *Geophysical Research Letters*, *44*, 12271–12279. https://doi.org/10.1002/2017GL075661

Rezvanbehbahani, S., Stearns, L. A., van der Veen, C. J., Oswald, G. K. A., & Greve, R. (2019). Constraining the geothermal heat flux in Greenland at regions of radar-detected basal water. *Journal of Glaciology*, *65*(254), 1023–1034. https://doi.org/10.1017/jog.2019.79

Rogozhina, I., Hagedoorn, J. M., Martinec, Z., Fleming, K., Soucek, O., Greve, R., & Thomas, M. (2012). Effects of uncertainties in the geothermal heat flux distribution on the Greenland ice sheet: An assessment of existing heat flow models. *Journal of Geophysical Research*, *117*, F02025. https://doi.org/10.1029/2011JF002098

Schaeffer, A., & Lebedev, S. (2013). Global shear speed structure of the upper mantle and transition zone. *Geophysical Journal International*, *194*(1), 417–449. https://doi.org/10.1093/gji/ggt095

Schaeffer, A., & Lebedev, S. (2015). Global heterogeneity of the lithosphere and underlying mantle: A seismological appraisal based on multimode surface-wave dispersion analysis, shear-velocity tomography, and tectonic regionalization. In *The Earth's heterogeneous mantle* (pp. 3–46). Springer. https://doi.org/10.1007/978-3-319-15627-9_1

Şengör, A. C., & Natal'in, B. A. (2001). Rifts of the world. *Geological Society of America Special Papers*, *352*, 389–482.

Seroussi, H., Ivins, E. R., Wiens, D. A., & Bondzio, J. (2017). Influence of a west Antarctic mantle plume on ice sheet basal conditions. *Journal of Geophysical Research: Solid Earth*, *122*, 7127–7155. https://doi.org/10.1002/2017JB014423

Shapiro, N. M., & Ritzwoller, M. H. (2004). Inferring surface heat flux distributions guided by a global seismic model: Particular application to Antarctica. *Earth and Planetary Science Letters*, *223*(1–2), 213–224. https://doi.org/10.1016/j.epsl.2004.04.011

Shen, W., Wiens, D. A., Anandakrishnan, S., Aster, R. C., Gerstoft, P., Bromirski, P. D., et al. (2018). The crust and upper mantle structure of central and west Antarctica from Bayesian inversion of Rayleigh wave and receiver functions. *Journal of Geophysical Research: Solid Earth*, *123*, 7824–7849. https://doi.org/10.1029/2017JB015346

Shen, W., Wiens, D. A., Lloyd, A. J., & Nyblade, A. A. (2020). A geothermal heat flux map of Antarctica empirically constrained by seismic structure. *Geophysical Research Letters*, *47*, e2020GL086955. https://doi.org/10.1029/2020GL086955

Stål, T., Reading, A. M., Halpin, J. A., & Whittaker, J. M. (2019). A multivariate approach for mapping lithospheric domain boundaries in East Antarctica. *Geophysical Research Letters*, *46*, 10404–10416. https://doi.org/10.1029/2019GL083453

Szwillus, W., Afonso, J. C., Ebbing, J., & Mooney, W. D. (2019). Global crustal thickness and velocity structure from geostatistical analysis of seismic data. *Journal of Geophysical Research: Solid Earth*, *124*, 1626–1652. https://doi.org/10.1029/2018JB016593

Van Liefferinge, B. (2018). *Thermal state uncertainty assessment of glaciers and ice sheets: Detecting promising oldest ice sites in Antarctica*.

van Wyk de Vries, M., Bingham, R. G., & Hein, A. S. (2018). A new volcanic province: An inventory of subglacial volcanoes in west Antarctica. *Geological Society, London, Special Publications*, *461*(1), 231–248. https://doi.org/10.1144/SP461.7

Williams, M. A., Kelsey, D. E., Hand, M., Raimondo, T., Morrissey, L. J., Tucker, N. M., & Dutch, R. A. (2018). Further evidence for two metamorphical events in the Mawson continent. *Antarctic Science*, *30*(1), 44–65. https://doi.org/10.1017/S0954102017000451

Winsborrow, M. C., Clark, C. D., & Stokes, C. R. (2010). What controls the location of ice streams? *Earth-Science Reviews*, *103*(1–2), 45–59. https://doi.org/10.1016/j.earscirev.2010.07.003

Youssof, M., Thybo, H., Artemieva, I., & Levander, A. (2013). Moho depth and crustal composition in southern Africa. *Tectonophysics*, *609*, 267–287. https://doi.org/10.1016/j.tecto.2013.09.001